FEBS Letters 589 (2015) 89–93

FEBS Letters

journal homepage: www.FEBSLetters.org

Pathogenic uromodulin mutations result in premature intracellular polymerization

Andrew P. Stewart [a,*], Richard N. Sandford [b], Fiona E. Karet Frankl [b], J. Michael Edwardson [a]

[a] Department of Pharmacology, University of Cambridge, Cambridge, United Kingdom
[b] Department of Medical Genetics, University of Cambridge, Addenbrooke's Hospital, Cambridge, United Kingdom

ARTICLE INFO

Article history:
Received 23 May 2014
Revised 31 October 2014
Accepted 19 November 2014
Available online 29 November 2014

Edited by Jesus Avila

Keywords:
Atomic force microscopy
Nephropathy
Protein polymerization
Uromodulin

ABSTRACT

Several renal diseases involve mutations in the gene encoding uromodulin, the predominant protein in urine. We investigated the intracellular processing of wild-type uromodulin, and three mutants: p.V93_G97del/ins AASC; C155R; and C150S. A renal biopsy from a patient harboring the C155R mutation revealed intracellular protein accumulation. Wild-type uromodulin was efficiently trafficked to the cell surface in transfected tsA 201 cells, whereas the mutants were partially retained within the cell, and incompletely processed. Atomic force microscopy imaging revealed that the intracellular mutant proteins contained fibrillar structures similar to urinary uromodulin. We suggest that premature intracellular polymerization underlies the pathology of uromodulin diseases.

1. Introduction

Uromodulin is the most abundant protein in human urine. A variety of functions have been ascribed to it, including modulation of water permeability of the nephron [1], prevention of bacterial colonization [2] and inhibition of urinary tract stone formation [3]. Mutations in *UMOD*, the gene that elaborates uromodulin, cause a number of allelic autosomal dominant renal diseases, including Familial Juvenile Hyperuricemic Nephropathy (FJHN) [4] and Medullary Cystic Kidney Disease (MCKD2) [5]. By a poorly-understood mechanism these diseases result in hyperuricemia, progressive tubulointerstitial fibrosis, a urinary concentrating defect and eventual renal failure requiring renal replacement therapy. Transplantation is curative. Interestingly, the *UMOD* locus has also been identified as the most significant in a genome-wide association study of all forms of chronic kidney disease (CKD) [6]. It has been suggested that increased expression levels associated with common variants at the *UMOD* locus might be the basis for this association [7].

It has been reported that some mutant forms of *UMOD* that result in autosomal dominant renal disease are retained within the endoplasmic reticulum (ER) in vitro, leading to a reduction in uromodulin secretion relative to wild-type (WT) [8–10]. This intracellular retention has also been seen in a transgenic mouse model of *UMOD* disease [11]. However, the structure of the secreted or retained protein has not previously been assessed. Here we used atomic force microscopy (AFM) imaging to investigate the structures of WT uromodulin, and of three disease-associated mutants: C155R (previously unreported), p.V93_G97del/ins AASC (Indel) [8] and C150S [12]. Our study provides the first evidence of structural defects resulting from pathological *UMOD* mutations, and suggests that *UMOD* pathology results from the premature intracellular polymerization of the mutant protein.

2. Materials and methods

2.1. Isolation of uromodulin from urine

With Ethical Committee approval (NRES 08-H0306-62), urine from three healthy human volunteers was centrifuged at 10000×*g* for 10 min, and the resulting pellet was resuspended in HEPES-buffered saline. Samples of urine and protein pellets were analyzed by SDS–polyacrylamide gel electrophoresis (SDS–PAGE),

Abbreviations: AFM, atomic force microscopy; CKD, chronic kidney disease; EM, electron microscopy; FJHN, Familial Juvenile Hyperuricemic Nephropathy; HA, hemagglutinin; MCKD, Medullary Cystic Kidney Disease; SDS–PAGE, SDS–polyacrylamide gel electrophoresis

* Corresponding author at: Department of Pharmacology, University of Cambridge, Tennis Court Road, Cambridge CB2 1PD, United Kingdom. Fax: +44 1223 334100.
E-mail address: aps54@cam.ac.uk (A.P. Stewart).

http://dx.doi.org/10.1016/j.febslet.2014.11.029
0014-5793/

followed by either Coomassie blue staining or immunoblotting using a sheep polyclonal anti-human uromodulin antibody (R&D Systems).

2.2. Cell culture

tsA 201 cells (a sub-clone of human embryonic kidney 293 cells stably expressing the SV40 large T-antigen) were grown in Dulbecco's modified Eagle's medium supplemented with 10% (v/v) fetal bovine serum, 100 μg/ml of streptomycin and 100 units/ml of penicillin in an atmosphere of 5% CO_2/air.

2.3. Constructs

WT human uromodulin, and the Indel (c.278_289del TCTGCCCCGAAGinsCCGCCTCCT; p.V93_G97del/ins AASC), C155R and C150S mutants, each bearing an N-terminal hemagglutinin (HA) epitope tag, were sequence-verified and expressed in the vector pcDNA3.1.

2.4. Immunofluorescence

Cells were transfected with DNA encoding one of the four HA-tagged uromodulin constructs (above). Cells were fixed, permeabilized and incubated with mouse monoclonal anti-HA primary antibody (Covance, HA.11 clone 16B12), followed by Cy3-conjugated goat anti-mouse secondary antibody. For double immunofluorescence experiments, uromodulin was detected using a rabbit polyclonal anti-HA antibody (Sigma), followed by a Cy3-conjugated goat anti-rabbit antibody (Sigma), and calnexin was detected using a mouse monoclonal antibody (Abcam, AF-18), followed by a fluorescein isothiocyanate-conjugated goat anti-mouse secondary antibody (Sigma). Cells were imaged by confocal laser scanning microscopy.

2.5. Isolation of epitope-tagged proteins

Using calcium phosphate precipitation, tsA 201 cells were transfected with 250 μg of DNA for 5 × 162 cm^2 flasks and incubated for 48 h at 37 °C to allow protein expression. Supernatant culture media were harvested, and cells were solubilized in 1% (v/v) Triton X-100 for 1 h at 4 °C. Samples were analyzed by immunoblotting using a mouse monoclonal anti-β-actin antibody (Sigma, clone AC-15). Both media and cell extracts were centrifuged at 62 000×*g* to remove all insoluble material. Clarified supernatants were incubated with anti-HA-agarose beads (Sigma) for 3 h. Beads were washed extensively and bound protein eluted with HA peptide (100 μg/ml). Eluted samples were analyzed by SDS–PAGE, followed by either immunoblotting using a mouse monoclonal anti-HA antibody, or Coomassie blue staining.

2.6. AFM imaging

Protein samples were diluted to a final concentration of 0.04 nM, and 45 μl of each sample was adsorbed to freshly cleaved mica disks for 5 min, followed by washing with Biotechnology Performance Certified-grade water (Sigma) and drying under nitrogen. Imaging was performed with a Veeco Digital Instruments Multimode atomic force microscope controlled by a Nanoscope IIIa controller. Samples were imaged in air, using tapping mode. The silicon cantilevers used had a drive frequency ~300 kHz and a specified spring constant of 40 N/m (Olympus). The applied imaging force was kept as low as possible ($A_s/A_0 \sim 0.85$). Fibrous structures were quantified using Scanning Probe Image Processor version 5 (Image Metrology).

2.7. Patients and clinical investigations

A diagnostic renal biopsy was obtained from the index case and processed for electron microscopy (EM) by standard methods. Genomic DNA from Kindred B was sequenced according to standard methods.

3. Results and discussion

Urine from a healthy volunteer was first analyzed by SDS–PAGE, followed by Coomassie blue staining or immunoblotting using an anti-uromodulin antibody. In both cases a major band was seen at ~95kDa (Fig. 1A), confirming the presence of uromodulin. Centrifugation of urine at 10 000×*g* for 10 min has been shown to pellet uromodulin [13]. As shown in Fig. 1B, the resuspended pellet contained uromodulin at an increased concentration and purity relative to the crude urine sample. Similar results were obtained with two additional healthy volunteers. The resuspended sample was imaged using AFM. Images showed the presence of large convoluted fibrous structures (Fig. 1C and D), and occasional circular features (arrowheads, Fig. 1C). Given that the uromodulin sample was essentially pure, we are confident that the fibrous structures do indeed represent uromodulin. Imaging of urine from a patient with FJHN caused by the Indel mutation revealed no obvious differences compared with WT, likely because of the presence of WT protein in the heterozygous condition (data not shown).

The index case in Kindred B (Fig. 2A) is a 35 year-old male who developed biochemical evidence of CKD at age 24 years. At that time he was hyperuricemic and suffering from recurrent gout, and allopurinol was commenced. Hypertension developed at age 25 years. His brother is currently under investigation for hyperuricemia with reduced urinary urate excretion, which is associated with *UMOD* nephropathy [4]. Their mother had pre-eclampsia during her first pregnancy. She also had CKD and hypertension since age 34 years; a recent estimated glomerular filtration rate

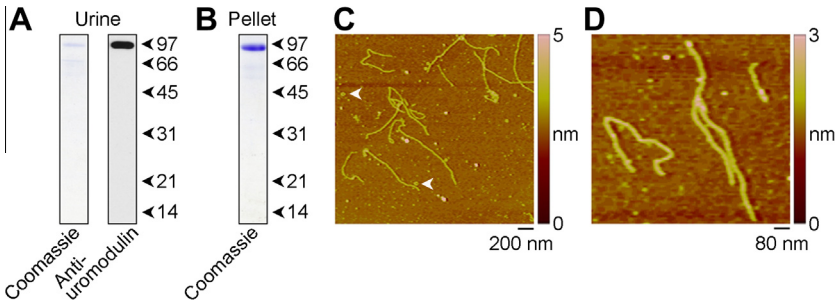

Fig. 1. Isolation and AFM imaging of uromodulin from human urine. (A) Healthy volunteer urine analyzed by SDS–PAGE followed by Coomassie blue staining or immunoblotting showed a major band at the expected molecular mass for uromodulin (~95kDa). Molecular mass markers (kDa) are shown. (B) Pelleted urinary protein consisted almost entirely of uromodulin. (C) A typical low-magnification AFM image of this uromodulin revealed large fibrous structures and occasional circular features (arrowheads). (D) High-magnification AFM image.

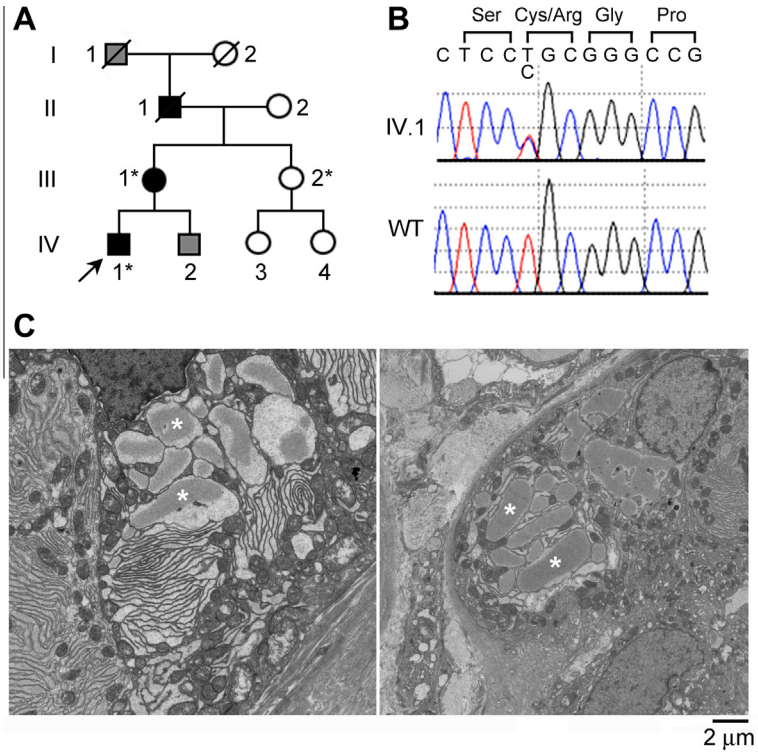

Fig. 2. Features of Kindred B. (A) Pedigree showing multi-generation history of renal disease (index case arrowed). Squares and circles denote males and females, respectively. White, black and gray symbols denote affected, unaffected and unknown status. *, genetically confirmed. (B) The lower sequence shows WT *UMOD*, and the upper sequence shows the C155R heterozygote, with the predicted amino acids indicated above. (C) Electron micrographs of a renal biopsy taken from the index case, showing marked protein accumulation in the ER and unstacking of Golgi cisternae (examples denoted by asterisks).

was 20, signifying CKD stage 4. The patient's maternal grandfather developed end-stage renal failure and died of complications of renal transplantation. Both the proband and his mother were found by direct genomic DNA sequencing to harbor the same heterozygous missense mutation (C155R) in *UMOD* (Fig. 2B). This is predicted to affect protein folding since (in common with most other reported mutations) it removes a cysteine residue [14]. No other potentially pathogenic sequence alterations were identified. Most patients with uromodulin nephropathy present with already-shrunken kidneys due to the progressive fibrotic process associated with the disorders, and as a consequence, renal biopsies are not performed. However, the C155R index patient has had a biopsy, which we were able to process for EM. Electron micrographs (Fig. 2C) show extensive accumulations of protein within the ER, and apparent unstacking and dilatation of the Golgi cisternae, indicating a severe intracellular trafficking defect with this *UMOD* mutant.

In order to study *UMOD* mutants in the absence of WT protein, constructs of WT, Indel, C155R and C150S uromodulin, each bearing an N-terminal HA tag, were generated. Note that Indel [8] is associated with a milder biochemical phenotype than the C155R or C150S [12] phenotypes. The four constructs were each transiently expressed in tsA 201 cells. Transfected cells were fixed, permeabilized and subjected to immunofluorescence analysis (Fig. 3A, upper panels). The majority of the WT protein was located at the plasma membrane. In contrast, C150S had a predominantly intracellular distribution, with clear accumulations of the protein inside the cell, rather than a diffuse reticular pattern. The Indel construct was of intermediate appearance, with reduced membrane staining and an increased intracellular signal, as previously demonstrated [8]. The novel C155R mutation had a staining pattern very similar to C150S, consistent with its severe phenotype in vivo, and also with the EM data. Higher-magnification images of intracellular compartments harboring the C150S mutant are shown in the lower panels (Fig. 3A). The staining pattern for the C150S mutant was compared with that for the recognized ER marker calnexin [15]. As can be seen (Fig. 3B), the immunofluorescence signals for the two proteins overlapped extensively, consistent with accumulation of C150S uromodulin in the ER.

Uromodulin was purified from either culture media of cells expressing the various constructs, or from Triton X-100-solubilized cell extracts, by anti-HA immunoaffinity chromatography. Identical conditions (i.e., volumes, dilutions, etc.) were used in each case, to permit direct comparisons of the extents of processing and secretion of the four forms of the protein. Immunoblotting of the Triton X-100 cell extracts for β-actin confirmed that equal amounts of protein were used as the starting material for the four purifications (Fig. 3C, top panel). Immunoblotting of equivalent samples of purified secreted protein with an anti-HA antibody showed a single band at ~95kDa, representing the mature, fully processed form of the protein (Fig. 3C, center-left panel). Notably, there was a progressive decrease in the quantity of secreted protein that correlated with the severity of the mutation; Coomassie blue staining confirmed this observation (Fig. 3C, bottom-left panel). Immunoblotting of the cellular protein revealed two bands at ~95kDa and ~85kDa, representing the mature, fully processed form seen in culture media and a smaller immature form, respectively (Fig. 3C, right panels) [8]. There was an increase in the proportion of immature protein with the mutants, particularly C155R and C150S, consistent with the intracellular retention profile reported above.

Uromodulin samples purified from the transfected tsA 201 cell supernatants and cell extracts were subjected to AFM imaging, and structural components quantified. Numerous fibrous structures were seen in the secreted WT sample (Fig. 4A). These were smaller and less convoluted than those found in urine, possibly because

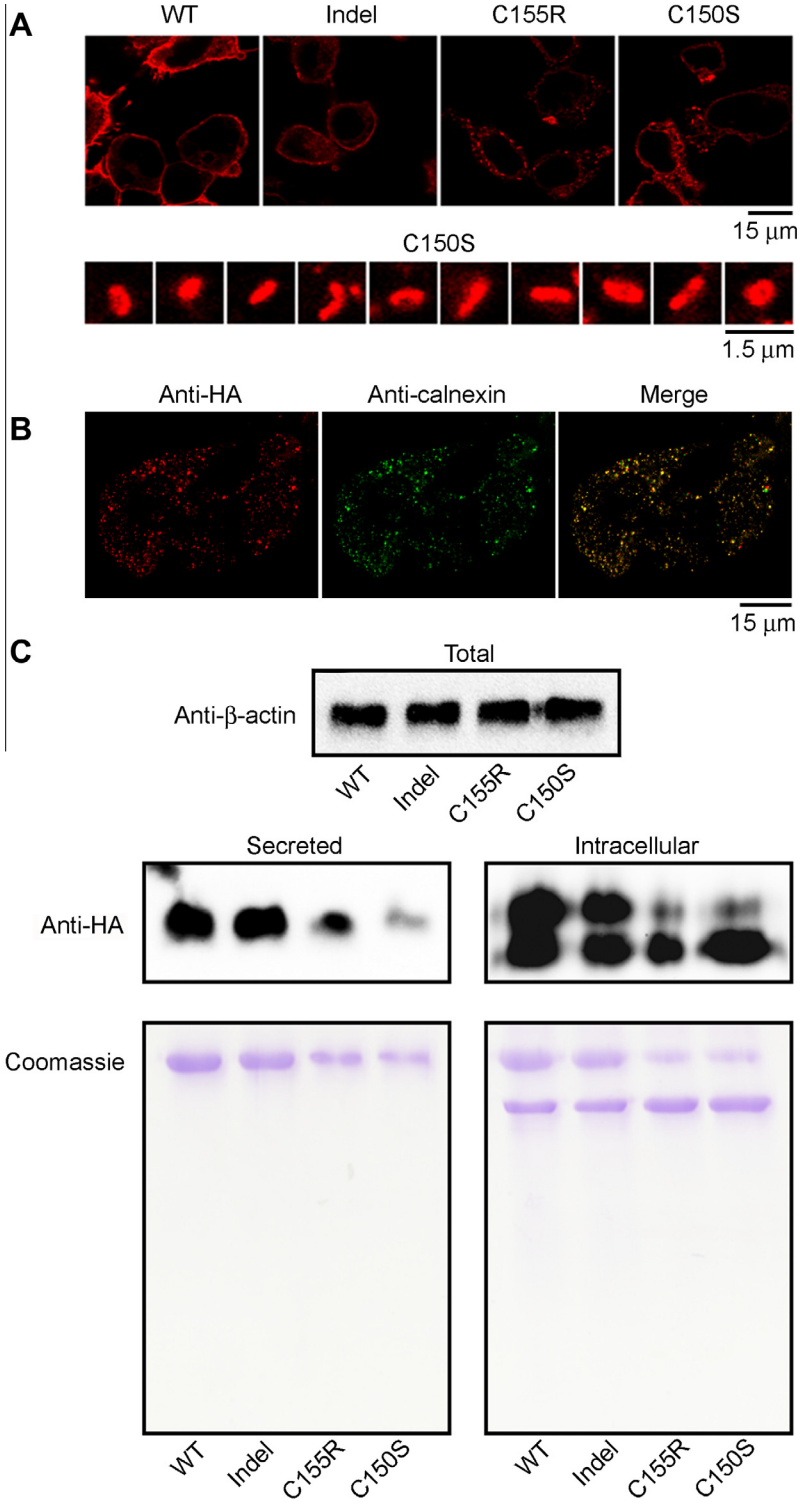

Fig. 3. Analysis of uromodulin trafficking and processing in transiently transfected tsA 201 cells. (A) WT protein was mostly at the plasma membrane (upper panels), while the mutants showed intracellular retention correlating with phenotypic severity. Zoomed images of intracellular aggregations seen in cells expressing C150S uromodulin are shown in the lower panels. (B) Immunofluorescence signals for C150S uromodulin and calnexin overlapped extensively, showing that the mutant uromodulin was predominantly localized in the ER. (C) Immunoblotting for β-actin showed that equal amounts of protein were present in the starting material for the four uromodulin purifications (top). HA-tagged uromodulin (WT, Indel, C155R and C150S) isolated from cell culture media (left) was composed of mature, fully processed uromodulin at ~95kDa, whereas detergent extracts of transfected cells (right) showed an additional ~85kDa band, representing immature protein.

they were secreted from transiently transfected cells or because the protein was isolated by binding to and elution from immunobeads. Significantly, despite lower secreted amounts, imaging of secreted samples from cells expressing the three uromodulin mutants showed no evidence of a structural abnormality, as similar fibrous structures were present in all three cases. This result demonstrates that while the three mutations cause intracellular protein retention, any protein that is secreted adopts a very similar

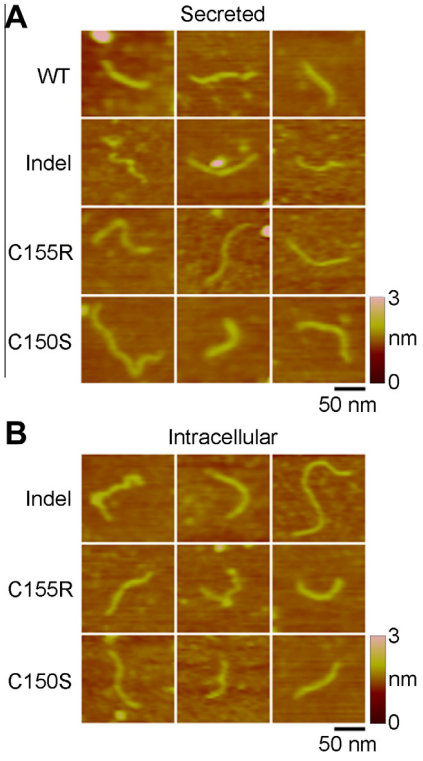

Fig. 4. AFM imaging of secreted and intracellular uromodulin. Zoomed images of typical fibrillar uromodulin structures seen for WT and mutants in cell culture media (A) and for mutants alone in cell extracts (B), indicating premature intracellular fibril assembly for the mutant proteins.

structure to WT. Importantly, very few fibrous structures (11 in 100 images) were seen in samples of purified intracellular WT uromodulin, indicating that polymerization normally occurs post-secretion. In marked contrast, all three mutant forms of uromodulin isolated from cell extracts contained numerous fibrous structures (Fig. 4B). Specifically, in 100 AFM images, the numbers of these structures were: 156 (Indel), 122 (C155R), and 110 (C150S). Hence, all three mutations cause abnormal, premature intracellular polymerization of uromodulin.

Our data suggest that *UMOD*-associated disease bears similarities to other intracellular protein aggregation disorders such as α_1-antitrypsin deficiency [16] and Parkinson's disease [17]. By analogy, chronic renal damage in patients carrying mutant *UMOD* could be explained by the activation of ER stress, overloaded or unfolded protein pathways, as described for these other conditions [18]. In conclusion, this study provides the first evidence that *UMOD* diseases result from inappropriate intracellular protein polymerization.

Acknowledgements

A.P.S. is a member of the University of Cambridge M.B./Ph.D. Programme, and was supported by the Jean Shanks Foundation and the James Baird Fund of the University of Cambridge. J.M.E., F.E.K. and R.N.S. are supported by Kidney Research U.K., and F.E.K. by the Cambridge Biomedical Research Centre. We are grateful to Dr. Vicky Bardsley for the electron micrographs, to Dr. Graham Smith for technical assistance and to Dr. Stefan Marciniak for useful discussions.

References

[1] Parsons, C.L., Bautista, S.L., Stein, P.C. and Zupkas, P. (2000) Cyto-injury factors in urine: a possible mechanism for the development of interstitial cystitis. J. Urol. 164, 1381–1384.
[2] Ørskov, I., Ferencz, A. and Ørskov, F. (1980) Tamm-Horsfall protein or uromucoid is the normal urinary slime that traps type 1 fimbriated *Escherichia coli*. Lancet 8173, 887.
[3] Mo, L., Huang, H.-Y., Zhu, X.-H., Shapiro, E., Hasty, D.L. and Wu, X.-R. (2004) Tamm-Horsfall protein is a critical renal defense factor protecting against calcium oxalate crystal formation. Kidney Int. 66, 1159–1166.
[4] Turner, J.J.O., Stacey, J.M., Harding, B., Kotanko, P., Lhotta, K., Puig, J.G., Roberts, I., Torres, R.J. and Thakker, R.V. (2003) UROMODULIN mutations cause familial juvenile hyperuricemic nephropathy. J. Clin. Endocrinol. Metab. 88, 1398–1401.
[5] Hateboer, N., Gumbs, C., Teare, M.D., Coles, G.A., Griffiths, D., Ravine, D., Futreal, P.A. and Rahman, N. (2001) Confirmation of a gene locus for medullary cystic kidney disease (MCKD2) on chromosome 16p12. Kidney Int. 60, 1233–1239.
[6] Köttgen, A., Glazer, N.L., Dehghan, A., Hwang, S.J., Katz, R., Li, M., Yang, Q., Gudnason, V., Launer, L.J., Harris, T.B., Smith, A.V., Arking, D.E., Astor, B.C., Boerwinkle, E., Ehret, G.B., Ruczinski, I., Scharpf, R.B., Chen, Y.D., de Boer, I.H., Haritunians, T., Lumley, T., Sarnak, M., Siscovick, D., Benjamin, E.J., Levy, D., Upadhyay, A., Aulchenko, Y.S., Hofman, A., Rivadeneira, F., Uitterlinden, A.G., van Duijn, C.M., Chasman, D.I., Paré, G., Ridker, P.M., Kao, W.H., Witteman, J.C., Coresh, J., Shlipak, M.G. and Fox, C.S. (2009) Multiple loci associated with indices of renal function and chronic kidney disease. Nat. Genet. 41, 712–717.
[7] Köttgen, A., Hwang, S.-J., Larson, M.G., Van Eyk, J.E., Fu, Q., Benjamin, E.J., Dehghan, A., Glazer, N.L., Kao, W.H., Harris, T.B., Gudnason, V., Shlipak, M.G., Yang, Q., Coresh, J., Levy, D. and Fox, C.S. (2010) Uromodulin levels associate with a common UMOD variant and risk for incident CKD. J. Am. Soc. Nephrol. 21, 337–344.
[8] Smith, G.D., Robinson, C., Stewart, A.P., Edwards, E.L., Karet, H.I., Norden, A.G., Sandford, R.N. and Karet Frankl, F.E. (2011) Characterization of a recurrent in-frame UMOD indel mutation causing late-onset autosomal dominant end-stage renal failure. Clin. J. Am. Soc. Nephrol. 6, 2766–2774.
[9] Williams, S.E., Reed, A.A.C., Galvanovskis, J., Antignac, C., Goodship, T., Kotanko, P., Lhotta, K., Morinière, V., Williams, P., Wong, W., Rorsman, P. and Thakker, R.V. (2009) Uromodulin mutations causing familial juvenile hyperuricaemic nephropathy lead to protein maturation defects and retention in the endoplasmic reticulum. Hum. Mol. Genet. 18, 2963–2974.
[10] Liu, M., Chen, Y., Liang, Y., Liu, Y., Wang, S., Hou, P., Zhang, H. and Zhao, M. (2013) Novel UMOD mutations in familial juvenile hyperuricemic nephropathy lead to abnormal uromodulin intracellular trafficking. Gene 531, 363–369.
[11] Bernascone, I., Janas, S., Ikehata, M., Trudu, M., Corbelli, A., Schaeffer, C., Rastaldi, M.P., Devuyst, O. and Rampoldi, L. (2010) A transgenic mouse model for uromodulin-associated kidney diseases shows specific tubulo-interstitial damage, urinary concentrating defect and renal failure. Hum. Mol. Genet. 19, 2998–3010.
[12] Bernascone, I., Vavassori, S., Di Pentima, A., Santambrogio, S., Lamorte, G., Amoroso, A., Scolari, F., Ghiggeri, G.M., Casari, G., Polishchuk, R. and Rampoldi, L. (2006) Defective intracellular trafficking of uromodulin mutant isoforms. Traffic 7, 1567–1579.
[13] Fernández-Llama, P., Khositseth, S., Gonzales, P.A., Star, R.A., Pisitkun, T. and Knepper, M.A. (2010) Tamm–Horsfall protein and urinary exosome isolation. Kidney Int. 77, 736–742.
[14] Rampoldi, L., Scolari, F., Amoroso, A., Ghiggeri, G. and Devuyst, O. (2011) The rediscovery of uromodulin (Tamm–Horsfall protein): from tubulointerstitial nephropathy to chronic kidney disease. Kidney Int. 80, 338–347.
[15] Wada, I., Rindress, D., Cameron, P.H., Ou, W.J., Doherty 2nd, J.J., Louvard, D., Bell, A.W., Dignard, D., Thomas, D.Y. and Bergeron, J.J. (1991) SSR alpha and associated calnexin are major calcium binding proteins of the endoplasmic reticulum membrane. J. Biol. Chem. 266, 19599–19610.
[16] Lomas, D.A., Evans, D.L., Finch, J.T. and Carrell, R.W. (1992) The mechanism of Z α_1-antitrypsin accumulation in the liver. Nature 357, 605–607.
[17] Arima, K., Uéda, K., Sunohara, N., Hirai, S., Izumiyama, Y., Tonozuka-Uehara, H. and Kawai, M. (1998) Immunoelectron-microscopic demonstration of NACP/α-synuclein-epitopes on the filamentous component of Lewy bodies in Parkinson's disease and in dementia with Lewy bodies. Brain Res. 808, 93–100.
[18] Roussel, B.D., Kruppa, A.J., Miranda, E., Crowther, D.C., Lomas, D.A. and Marciniak, S.J. (2013) Endoplasmic reticulum dysfunction in neurological disease. Lancet Neurol. 12, 105–118.